Electronic Supplementary Material (ESI) for Nanoscale.

Electronic Supplementary Information

Growth of Copper Oxide Nanocrystals in Metallic Nanotube for High Performance Battery Anode

Yuxin Zhao, [a,b] Shanjun Mu,[b] Wanfu Sun,[b] Quanzhen Liu,[b] Yanpeng Li,[c] Zifeng Yan,[c] Ziyang Huo*[d] and Wenjie Liang*[a]

[a] *Beijing National Laboratory for Condensed Matter Physics, Beijing Key Laboratory for Nanomaterials and Nanodevices,Institute of Physics, Chinese Academy of Sciences, No.8, 3rd South Street, Zhongguancun, Haidian District, Beijing, 100190, China.*
[b] *State Key Laboratory of Safety and Control for Chemicals, SINOPEC Safety Engineering Institute, No 218, Yan'an 3 road, Shinan District, Shandong, Qingdao, 266071, China.*
[c] *State Key Laboratory for Heavy Oil Processing, PetroChina Key Laboratory of Catalysis, China University of Petroleum, Qingdao 266580, China.*
[d] *Queensland Micro- and Nanotechnology Centre Nathan campus, Griffith University, 170 Kessels Road, NATHAN QLD 4111 Australia.*

Supporting information to DOI 10.1039/x0xx00000x

SUPPORTING FIGURES

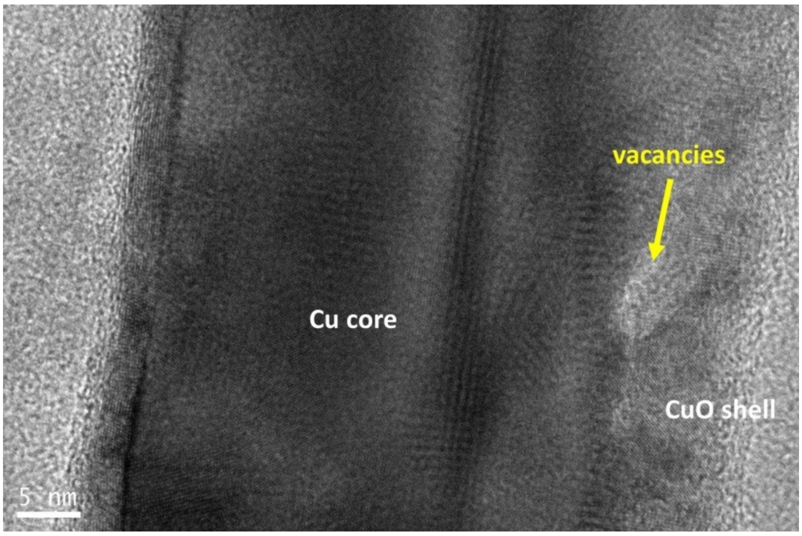

Figure S1. HRTEM images of the vacancies generated at the Cu/CuO interface.

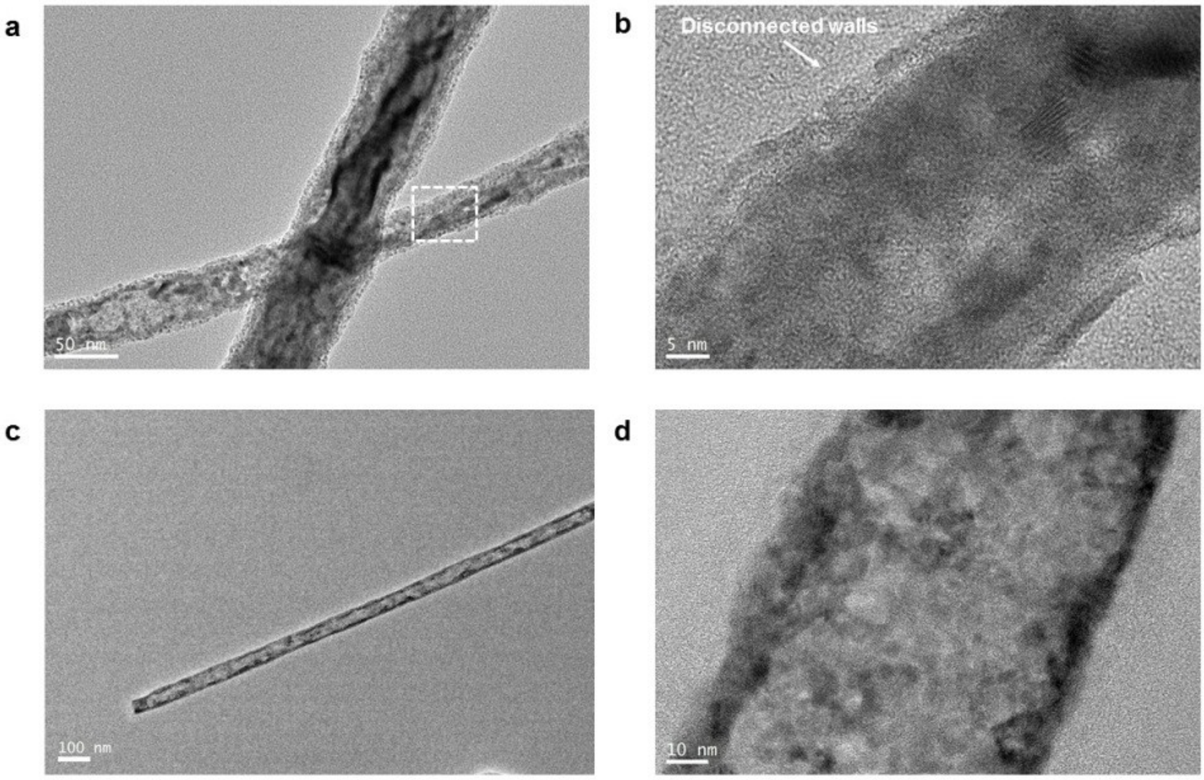

Figure S2. For reaction temperatures between 60 °C and 300 °C, the fundamental mechanisms would not change while only the reaction rate increases. Changing the reaction temperature therefore only results in the formation of hollow nanostructures throughout the entire NW instead of the desired semi-hollow structures. a) TEM images of CuO nanostructure with intermittent columns obtained after exposure process at lower temperature (50 ºC). b) HRTEM image of selected area in a, which reveals discontinuous outer walls. c) TEM images of CuO NT after exposure process at higher temperature (100 ºC). d) HRTEM image of a section from CuO NT.

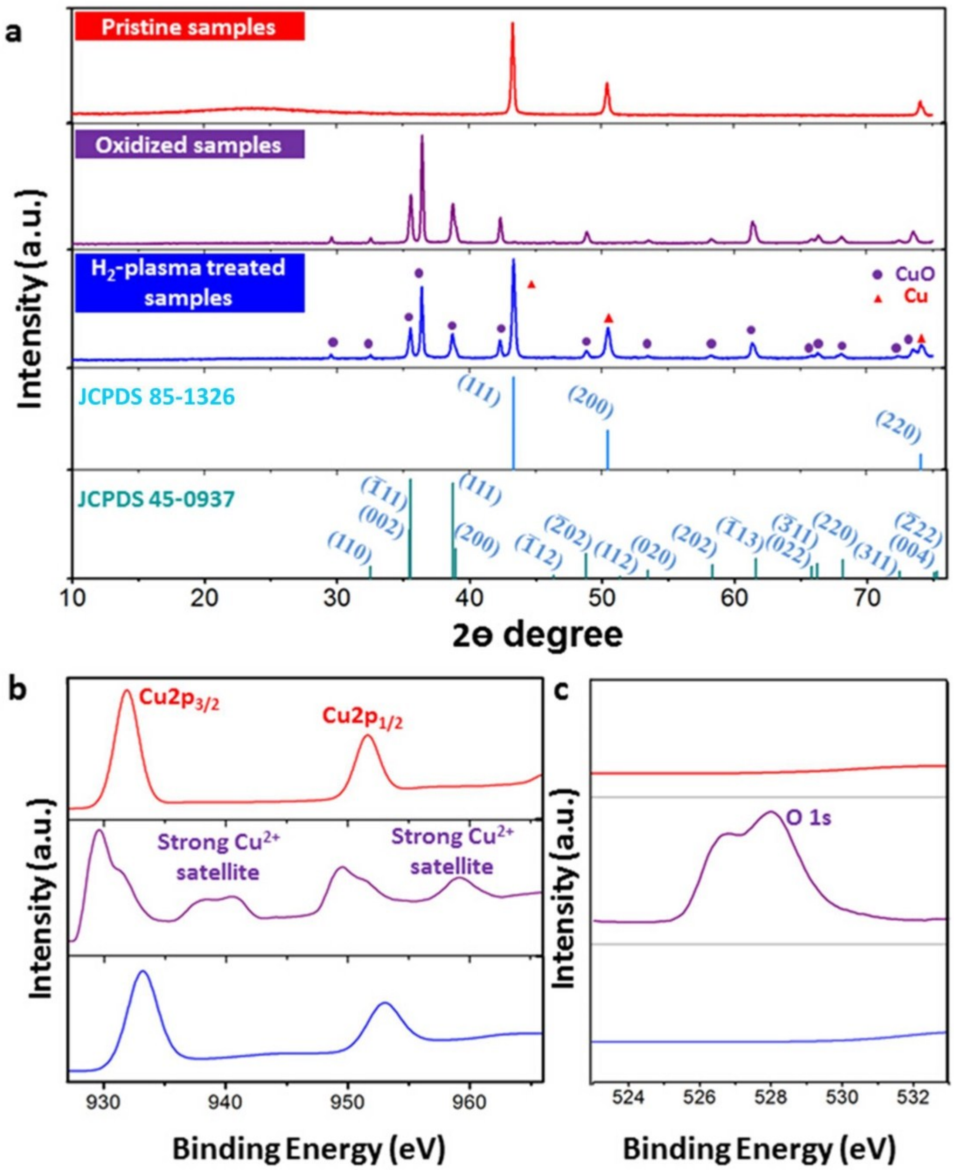

Figure S3. a) XRD patterns of pristine NWs (red), sample after oxidation process (purple) and final product after H_2 plasma treatment (blue). b, c) Corresponding XPS spectra of the Cu 2p and O 1s regions of these samples, respectively.

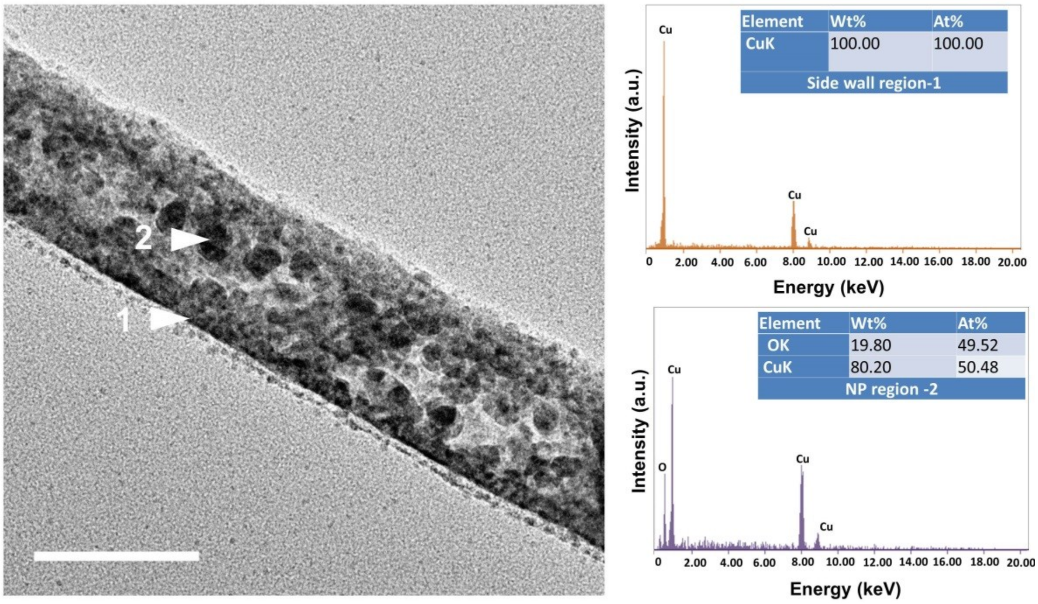

Figure S4. EDS spectra captured from the side wall region and NP region of the CuO-NPs@Cu NT as indicated in position 1 and 2.

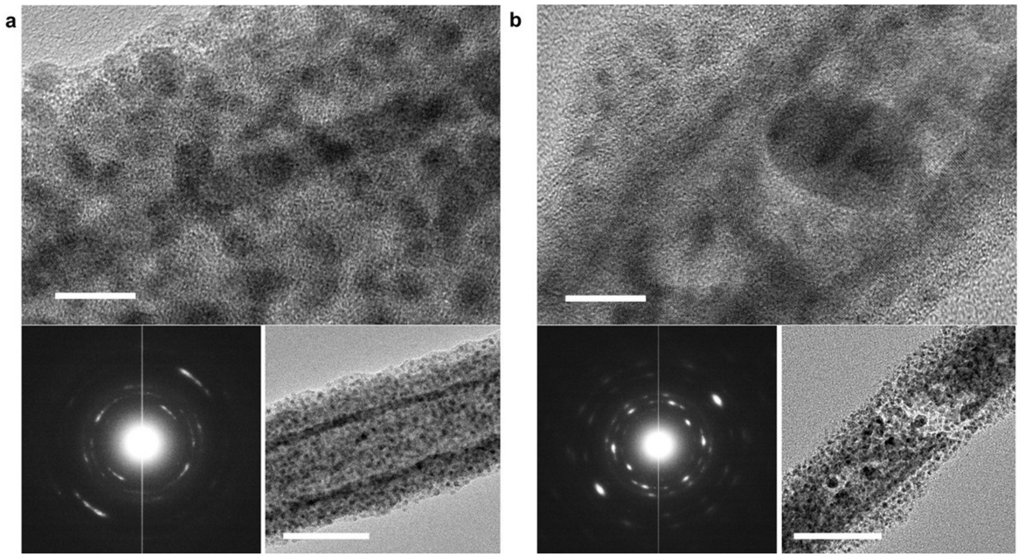

Figure S5. High-resolution TEM images reveal the porosity of degraded walls: a) CuO NT; b) CuO-NPs@CuO NT. Scale bars are 5 nm. The insets show their corresponding SAED patterns and bright field TEM image of the corresponding incomplete tube structure (scale bars: 50 nm).

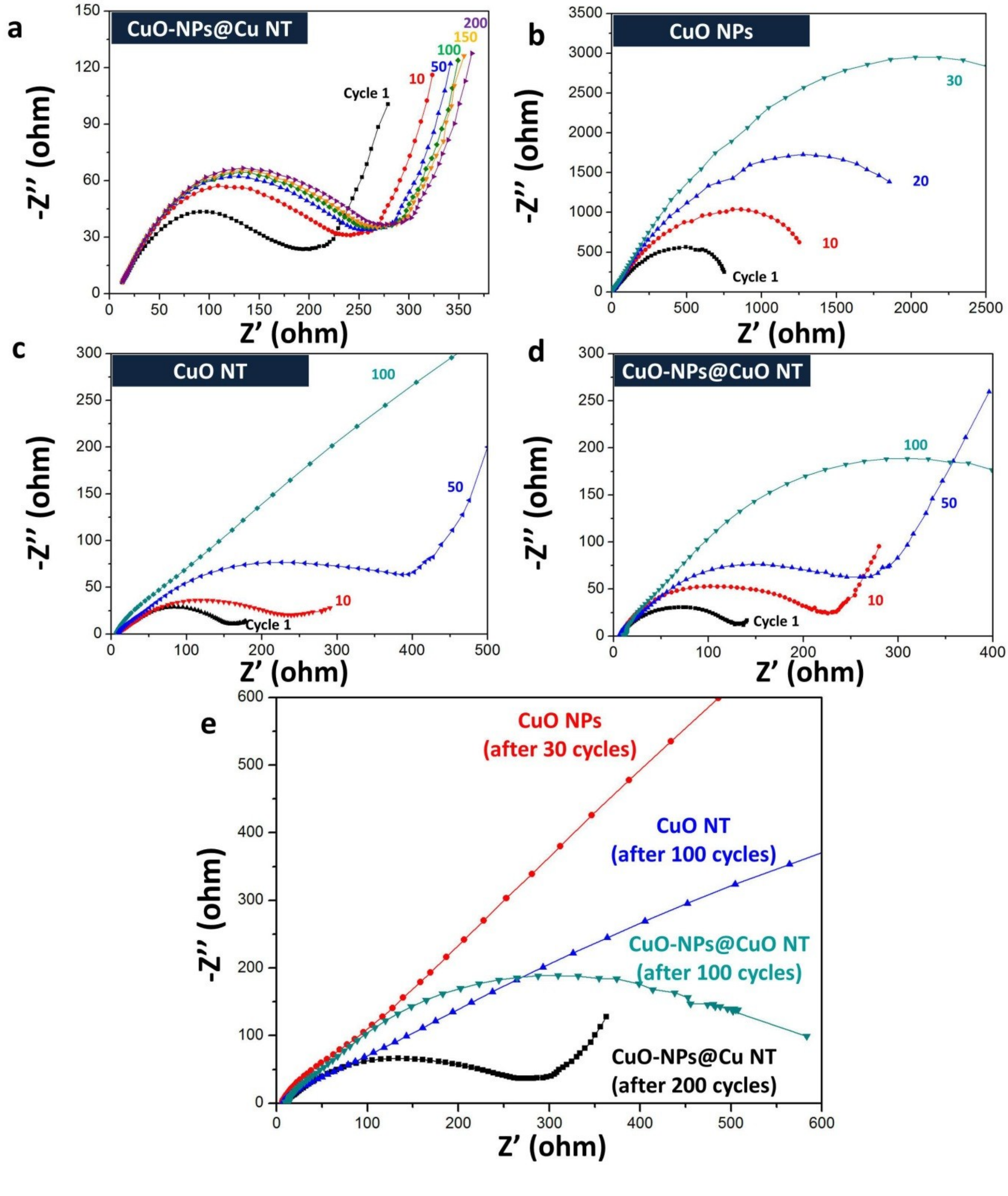

Figure S6. a) Cell impedance tests of the CuO-NPs@Cu NT electrode after 1st, 10th, 50th, 100th, 150th and 200th deep cycles. b-d) Electrochemical impedance spectroscopy of b) CuO NPs, c) CuO NT, and d) CuO-NPs@CuO NT anodes after different cycles. e) Comparison of electrochemical impedance spectroscopies between CuO-NPs@Cu NT electrode and reference electrodes after cycling tests.

Figure S7. A digital photo of CuO-NPs@Cu NTs solution (30 grams, dispersed in 400 mL methanol) in a 1 L glass container.

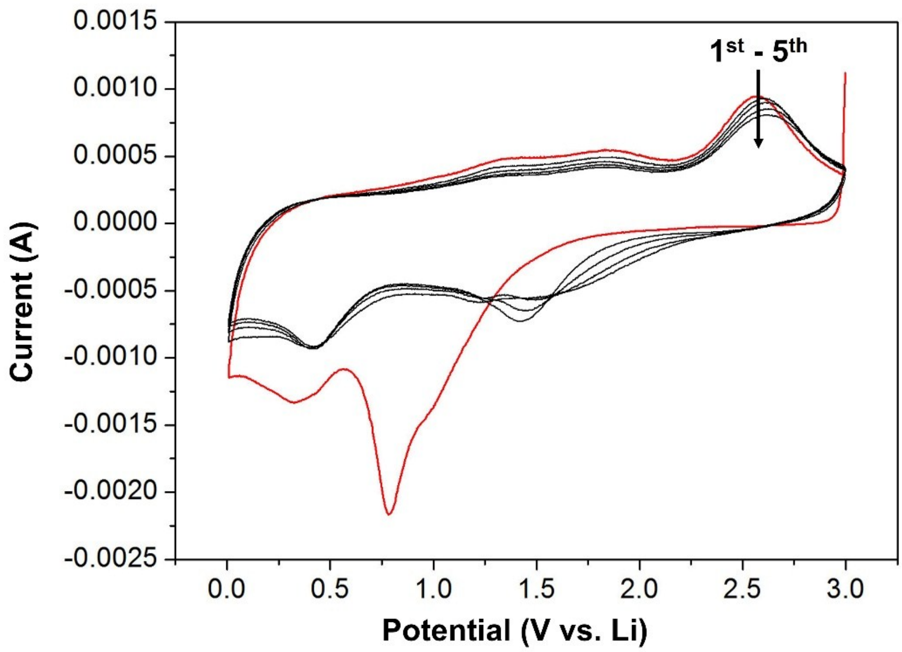

Figure S8. Cyclic voltammograms (CV) of CuO-NPs@Cu NT cell cycled between 0.02~3 V vs. Li at a scan rate of 5 mV/s. This result reveals that the first scan curve differed significantly from subsequent four cycles, and the overlapping of 2^{nd}~5^{th} cycling traces is noted during both cathodic and anodic sweeps, which corresponds to the stability of CuO during lithium cycling. In the cathodic sweep the cell showed a weaker broad peak ~2.17 V vs. Li which corresponds to the solid solution formation (Li_xCuO). Another two sharp peaks around ~1.29 and ~0.38V vs. Li are associated with the generation of Cu_2O, following further reduction into Cu^o and amorphous Li_2O. This is consistent with the galvanostatic charge/discharge voltage profiles illustrated in Figure 3c.

Table S1. Comparison of various CuO-based nanostructures electrochemical performances as anode for Li-ion battery

Type of CuO-based nanostructures	Reversible capacities for first ($mAhg^{-1}$)	Capacity fading after cyclic test ($mAhg^{-1}$ per cycle)	Number of cycles	C-rate or current density	Ref.
CuO nanodisc/MWCNT	657	10.85	20	134 mAg^{-1}	1
CuO hollow microspheres	750	<3	50	0.2 C	2
CuO/C hollow spheres	560	2.4	50	100 mAg^{-1}	3
CuO hierarchical hollow micro/nanostructures	~560	13	20	0.1 C	4
Pillow shaped CuO	~370	1	50	67 mAg^{-1} (0.1 C)	5
Ultrafine CuO NWs	680	7	30	67 mAg^{-1} (0.1 C)	6
CuO nanoribbons	495	-0.41	275	100 mAg^{-1}	7
CuO/graphene	561	2.76	50	67 mAg^{-1}	8
CuO NFs	453	0.26	100	100 mAg^{-1}	9
Cu@Cu_2O@CuO NS-NWs	674	0.21	100	100 mAg^{-1}	10
CuO-HM	525.2	<0.2	500	67 mAg^{-1}	11
CuO/Cu/C NFs	572	0.03	500	500 mAg^{-1}	12
CuO-NPs@Cu NT	**607**	**0.18**	**200**	**100 mAg^{-1}**	**This study**

NW-nanowire; NS-nanosheet; MWCNT- multi walled carbon nanotube; NF-nanofiber; HM-hierarchical CuO mesocrystals.

Table S2. Comparison of various CuO-based nanostructures rate capacity performances as anode for Li-ion battery

Type of Cu_xO-based nanostructures	minimum current density (mAg^{-1})	Capacities at minimum current density ($mAhg^{-1}$)	maximum current density (mAg^{-1})	Capacities at maximum current density ($mAhg^{-1}$)	Ref.
porous CuO NRs	300	654	3600	410	13
CuO/Cu_2O hollow polyhedrons	100	480	1600	130	14
CuO NFs	100	453	222	167	9
MOF derived CuO nanostructures	50	600	2000	210	15
CuO/C hollow spheres	100	560	1000	165	3
Ultrafine CuO NWs	67	760	1072	420	6
CuO nanoribbons	100	594	800	332	7
mesoporous CuO particles/CNT	120	590	18000	120	16
CuO/Cu/C NFs	500	561	6000	235	12
CuO-NPs@Cu NT	100	607	15000	175	This study

NRs-nanorods; NFs-nanofibers; NWs-nanowires; NS-nanosheet; CNT-carbon nanotube

References

[1] S.-D. Seo, Y.-H. Jin, S.-H. Lee, H.-W. Shim and D.-W. Kim, *Nanoscale Research Letters*, 2011, **6**, 397.

[2] S. Q. Wang, J. Y. Zhang and C. H. Chen, *Scripta Materialia*, 2007, **57**, 337-340.

[3] X. H. Huang, C. B. Wang, S. Y. Zhang and F. Zhou, *Electrochimica Acta*, 2011, **56**, 6752-6756.

[4] S. Gao, S. Yang, J. Shu, S. Zhang, Z. Li and K. Jiang, *The Journal of Physical Chemistry C*, 2008, **112**, 19324-19328.

[5] M. Wan, D. Jin, R. Feng, L. Si, M. Gao and L. Yue, *Inorganic Chemistry Communications*, 2011, **14**, 38-41.

[6] F. Wang, W. Tao, M. Zhao, M. Xu, S. Yang, Z. Sun, L. Wang and X. Song, *Journal of Alloys and Compounds*, 2011, **509**, 9798-9803.

[7] F.-S. Ke, L. Huang, G.-Z. Wei, L.-J. Xue, J.-T. Li, B. Zhang, S.-R. Chen, X.-Y. Fan and S.-G. Sun, *Electrochimica Acta*, 2009, **54**, 5825-5829.

[8] Y. J. Mai, X. L. Wang, J. Y. Xiang, Y. Q. Qiao, D. Zhang, C. D. Gu and J. P. Tu, *Electrochimica Acta*, 2011, **56**, 2306-2311.

[9] R. Sahay, P. Suresh Kumar, V. Aravindan, J. Sundaramurthy, W. Chui Ling, S. G. Mhaisalkar, S. Ramakrishna and S. Madhavi, *The Journal of Physical Chemistry C*, 2012, **116**, 18087-18092.

[10] Y. Zhao, Y. Zhang, H. Zhao, X. Li, Y. Li, L. Wen, Z. Yan and Z. Huo, *Nano Res.*, 2015, **8**, 2763-2776.

[11] X. Duan, H. Huang, S. Xiao, J. Deng, G. Zhou, Q. Li and T. Wang, *Journal of Materials Chemistry A*, 2016, **4**, 8402-8411.

[12] H. Zhang, G. Zhang, Z. Li, K. Qu, L. Wang, W. Zeng, Q. Zhang and H. Duan, *Journal of Materials Chemistry A*, 2016, **4**, 10585-10592.

[13] L. Wang, H. Gong, C. Wang, D. Wang, K. Tang and Y. Qian, *Nanoscale*, 2012, **4**, 6850-6855.
[14] L. Hu, Y. Huang, F. Zhang and Q. Chen, *Nanoscale*, 2013, **5**, 4186-4190.
[15] S. Venkatachalam, H. Zhu, C. Masarapu, K. Hung, Z. Liu, K. Suenaga and B. Wei, *ACS Nano*, 2009, **3**, 2177-2184.
[16] S. Ko, J.-I. Lee, H. S. Yang, S. Park and U. Jeong, *Advanced Materials*, 2012, **24**, 4451-4456.